

# Flow of Polar and Nonpolar Liquids through Nanotubes: A Computational Study

Andrii Kyrylchuk<sup>1,2</sup> and David Tománek<sup>1,\*</sup>

<sup>1</sup>*Physics and Astronomy Department, Michigan State University, East Lansing, Michigan 48824-2320, USA*

<sup>2</sup>*Institute of Organic Chemistry, National Academy of Sciences of Ukraine, Murmanska Str. 5, 02660 Kyiv, Ukraine*

(Dated: Wednesday 30<sup>th</sup> June, 2021)

We perform *ab initio* density functional calculations to study the flow of water, methanol and dimethyl ether through nanotubes of carbon and boron nitride with different diameters and chiralities. The liquids we choose are important solvents, with water and methanol being polar and dimethyl ether being non-polar. In terms of activation barriers for liquid transport, we find the molecular-level drag to decrease with decreasing nanotube diameter, but to be rather independent of the chiral index. We also find molecules with higher polarity to experience higher drag during the flow. Counter-intuitively, we find the drag for water in boron nitride nanotubes not to exceed that in carbon nanotubes due to frustration in competing long-range Coulomb interactions.

## I. INTRODUCTION

The field of micro- and nanofluidics has been evolving rapidly during the last decades, with its broad impact ranging from medical devices [1–3] to advanced fabrics and energy conversion devices [4–6] and advanced membranes for water desalination by reverse osmosis [7]. Aligned carbon nanotube (CNT) membranes attract much interest because of their well-defined pore size, their capability to form composite matrices [8] and their resistance to biofouling [9]. Many useful properties of CNTs are also found in related BN nanotubes (BNNTs) formed of hexagonal boron nitride [10]. These benefits combined with high thermal, chemical and mechanical stability should make CNTs and BNNTs a very suitable material to form membranes [8]. Consequently, understanding the flow of fluids inside nanometer-sized channels in these nanotubes is of growing importance [11].

Since liquid flow inside nanotubes could not be observed with sub-nanometer resolution so far, our understanding to date has relied almost exclusively on molecular dynamics (MD) simulations. Many force fields have been developed to describe the delicate interplay among the strong and weak forces that determine the behavior of liquids including water [6, 12–16], but none has been able to satisfactorily reproduce all aspects of their behavior including their interaction with solids in an unbiased manner. Such calculations provide valuable information, but final results depend heavily on models used for interatomic interactions, including the flexibility of bond lengths and angles in water, molecular polarizability and long-range electrostatic interactions [6, 16]. On the other hand, force fields based on *ab initio* total energy functionals including DFT are nominally free of adjustable parameters, but high computational requirements have severely limited their use.

Much insight has been obtained so far using different types of MD simulations. Occurrence of water wires inside small CNTs has been revealed by model force

field simulations [12–15]. These results were confirmed by *ab initio* density functional theory (DFT) calculations [17, 18] and Raman spectroscopy observations [19]. Formation of stacked ring structures in wide CNTs with diameters  $\gtrsim 10$  Å has been corroborated by MD simulations based on model force fields [14, 20–22] and DFT [23]. These findings were experimentally confirmed by IR spectroscopy [24] and X-ray diffraction [25]. Still, there are very many open questions [11].

There is some experimental evidence [26–30] that the flow velocity of liquids inside nanometer-sized pores is several orders of magnitude higher than what conventional theory based on Newtonian flow and the Hagen-Poiseuille equation would predict [31]. There are clearly some pitfalls in the way to translate and interpret experimental data into microscopic fluid flow speeds [7]. In particular, slip-flow of liquids inside nanochannels of different types needs to be addressed. To date there are no conclusive experimental or parameter-free *ab initio* results regarding the dependence of fluid flow inside nanotubes in terms of nanotube type, diameter and chirality. Still there are many questions to be addressed regarding mass transport of liquids through nanotubes and nanopores in general.

In this manuscript we address atomic-scale details of the flow of water, methanol and dimethyl ether through nanotubes of carbon and boron nitride with different diameters and chiralities. These liquids are important solvents, with water and methanol being polar and dimethyl ether being non-polar. We determine the potential energy of isolated molecules along the inner nanotube surface to determine activation barriers for diffusion, which translate into molecular-level drag. We find this drag to decrease with decreasing nanotube diameter, but to be rather independent of the chiral index. We also find that molecules with higher polarity experience higher drag during the flow.

---

\* E-mail: [tomanek@msu.edu](mailto:tomanek@msu.edu)

## II. COMPUTATIONAL APPROACH

Our computational approach to study liquid water and other solvents interacting with carbon nanotubes is based on *ab initio* density functional theory (DFT) as implemented in the SIESTA [32] code. Unless specified otherwise, we used the nonlocal Perdew-Burke-Ernzerhof (PBE) [33] exchange-correlation functional, norm-conserving Troullier-Martins pseudopotentials [34], a double- $\zeta$  basis including polarization orbitals, and a mesh cutoff energy of 500 Ry to determine the self-consistent charge density. We have used periodic boundary conditions throughout the study, with nanotube separated by  $\gtrsim 9$  Å vacuum space. Since the nanotube unit cells were long, we sampled the reciprocal space by a uniform  $1 \times 1 \times 2$   $k$ -point grid [35]. Systems with very large unit cells have been represented by the  $\Gamma$  point only. This provided us with a precision in total energy of  $\lesssim 2$  meV/atom. Geometries have been optimized using the conjugate gradient (CG) method [36], until none of the residual Hellmann-Feynman forces exceeded  $10^{-2}$  eV/Å. While computationally rather demanding, the DFT-PBE total energy functional is free of adjustable parameters and has been used extensively to provide an unbiased description water and its interaction with solids [23, 37]. Selected MD simulations were performed using 0.3 fs time steps, which were sufficiently short to guarantee energy conservation in a microcanonical ensemble.

## III. RESULTS

As mentioned above, the vast majority of atomistic MD simulations is based on parameterized force fields, which offer high degree of numerical efficiency and allows to study the motion of several thousand atoms simultaneously. The drawback of this approach is its lack of universality and quantitative predictability: force fields optimized for bulk fluids need to be changed at interfaces and in situations, where long-range electrostatic interactions play a role [6, 16]. For this reason, we decided to use the *ab initio* DFT formalism in our study. In spite of its high computational demand, DFT is nominally free of parameters and independent of predefined assumptions. This approach has been validated in successfully predicting static and dynamic properties of liquid water [7] and should provide valuable information that should complement large-scale studies with parameterized force fields.

Since DFT poses serious limitations on the number of atoms in the unit cell, small system sizes used in DFT calculations increase the statistical noise and thus limit quantitative conclusions. To avoid this problem, our following results are obtained using static calculations rather than MD simulations. As a good indication of the drag, which molecules experience at the interface during flow through narrow cavities, we calculated the potential energy of a single molecule drifting along nanotubes

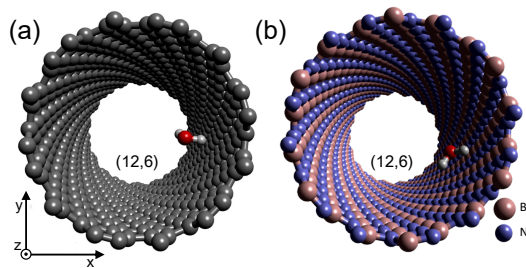


FIG. 1. A (12,6) chiral nanotube of (a) carbon and (b) boron nitride (BN), containing one water molecule.

with different composition, diameters, and chiral indices. These results reveal potential energy barriers that should correlate with the friction coefficients and slip lengths. We oriented the nanotube axis along the  $z$ -direction and fixed all nanotube atoms in their relaxed positions. We then determined the interaction energy between the enclosed molecule  $M$  and the nanotube, defined by

$$\Delta E = E_{tot}(M@NT) - E_{tot}(M) - E_{tot}(NT). \quad (1)$$

A negative value of  $\Delta E$  indicates an energetic preference for  $M$  to be inside rather than to be isolated from the nanotube.  $\Delta E(z)$  was calculated along the diffusion path of the molecule by fixing only the  $z$ -coordinate of a representative atom and relaxing all remaining molecular degrees of freedom, starting with the molecule close to the inner nanotube surface. This approach leaves the molecule free to find its optimum position within the  $x-y$  plane normal to the tube axis, to optimize its shape and orientation. We considered a result to be converged when the same final geometry with the same energy was reached from different starting positions. The full  $\Delta E(z)$  potential energy surface was obtained by a sequence of steps involving displacements of the representative atom along the tube axis. The ‘step size’ was determined by the length of the nanotube unit cell, which depends solely on the chiral index. In our calculations we used step sizes ranging from 0.2 . . . 1.0 Å.

### A. Water interactions with CNTs

Our first study was dedicated to the interaction of individual water molecules with a CNT and a BNNT. The position of the  $H_2O$  molecule along the tube axis, which is parallel to the  $z$ -axis, is represented the  $z$ -coordinate of the oxygen atom. ‘Snap shots’ of a water molecule inside the (12,6) CNT and BNNT are shown in Fig. 1.

Quantitative results for  $E(z)$  for water inside an armchair (8,8) and a zigzag (14,0) CNTs with essentially the same diameter  $d = 11.0$  Å are presented in Fig. 2. We have optimized the  $H_2O$  molecule using two starting configurations, with the CNT inner wall facing either the H-atoms ( $H_2O$ -H/CNT) or facing the oxygen ( $H_2O$ -O/CNT). Chemical intuition suggests a repulsion

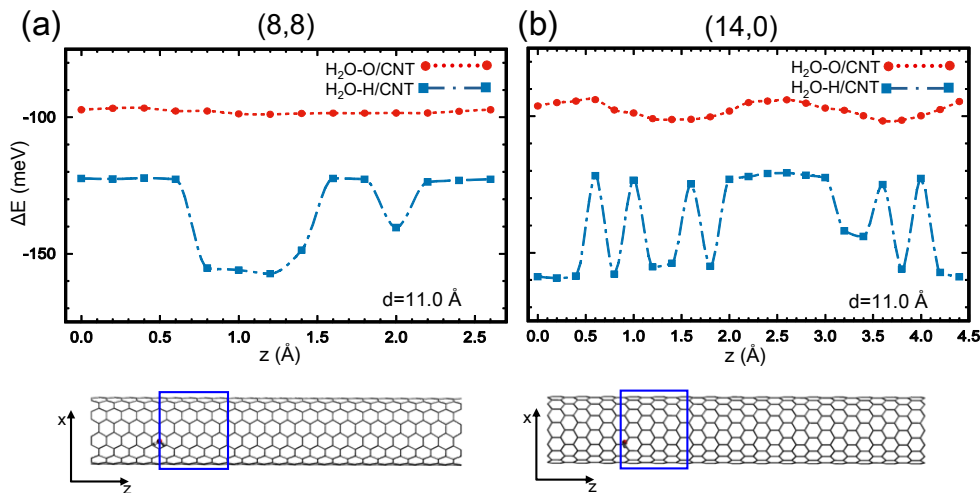


FIG. 2. Interaction energy  $\Delta E(z)$  between an isolated  $\text{H}_2\text{O}$  molecule and a surrounding (a) armchair (8,8) and (b) zigzag (14,0) CNT. The range of  $\Delta E(z)$  values is the same in both panels. The  $z$ -coordinate represents the water position along the  $z$ -axis of the CNT. We distinguish  $\text{H}_2\text{O}$ -H/CNT configuration, where H-end of  $\text{H}_2\text{O}$  faces the wall, from  $\text{H}_2\text{O}$ -O/CNT, where the O-end faces the wall. Negative values of  $\Delta E$  indicate energetic preference for  $\text{H}_2\text{O}$  entering the nanotube. The lower panels give a schematic view of the respective nanotubes. Nanotube diameters  $d$  are indicated in the individual panels. The size of the unit cell considered is outlined by the blue box.

between the oxygen lone electron pairs and the  $\pi$ -system of the CNT, pushing the molecule toward the center. The small positive charge on the hydrogen atoms, on the other hand, should attract the molecule towards the wall. This is confirmed by our results in Fig. 2(a): A water molecule gains  $\lesssim 98.9$  meV when entering an (8,8) CNT with oxygen facing the wall and as much as  $\approx 157.3$  meV when the hydrogens face the wall. Of these two configurations, the one with oxygen facing the wall is metastable. As seen in Fig. 2(b), we find roughly the same binding energies for the two configurations in the (14,0) CNT with the same diameter.

The weaker interaction of the metastable configuration with O facing the wall also results in a very weak dependence of  $\Delta E(z)$  on the position of the molecule both in the (8,8) and in the (14,0) CNT. In this orientation,  $\text{H}_2\text{O}$  may slip along the CNT wall with essentially no barrier. The situation is different in the stable configuration of water facing the CNT wall with its hydrogen atoms. Besides a higher binding energy in this orientation, also the barriers in  $\Delta E(z)$  are significantly higher, of the order of 40 meV. The precise position of the minima and maxima results from the hydrogen pair in  $\text{H}_2\text{O}$  finding a match or a mismatch with C atoms in the graphitic CNT wall. Especially in wide CNTs, the range of  $\Delta E(z)$  values is approximately the same independent of chirality, since it essentially represents the interaction of a water molecule with a graphene layer. It is only the sequence of minima and maxima that distinguishes between chiral indices in the same way as different sequences of maxima and minima occur when a water molecule crosses a graphene sheet along different trajectories.

In the following investigations, we will only consider the stable configuration of  $\text{H}_2\text{O}$  molecules facing the nan-

otube wall with their hydrogen atoms.

## B. Water diffusion inside zigzag and armchair CNTs

We display the potential energy surface  $\Delta E(z)$  for water diffusion inside CNTs with selected chiral indices in Fig. 3. A more complete list of potential energy barriers  $E_p$  is presented in Table I. As a general trend, we notice that the size of the diffusion barriers decreases with decreasing CNT diameter. We also find that the  $\text{H}_2\text{O}$ -CNT interaction increases with decreasing nanotube diameter, making narrower CNTs more hydrophilic. Thus, with decreasing tube diameter  $d$ , CNTs turn from hydrophobic ( $d \rightarrow \infty$  for graphene) to increasingly hydrophilic and eventually to hydrophobic at diameters too small to accommodate a water molecule. The increase of the  $\text{H}_2\text{O}$ -CNT interaction and reduction of activation barriers is

TABLE I. Energy barriers  $E_p$  for the diffusion of an isolated  $\text{H}_2\text{O}$  molecule along CNTs with a specific chiral index and diameter  $d$ . Reported results are for orientation of the molecule with its hydrogen pair facing the wall.

Chiral Index	$d$ (Å)	$E_p$ (meV)
(5,5)	6.8	2.8
(6,6)	8.1	1.5
(10,0)	7.8	4.9
(8,8)	11.0	35.0
(14,0)	11.0	38.5
(10,6)	11.0	37.6
(11,5)	11.1	36.5
(12,3)	10.8	37.3

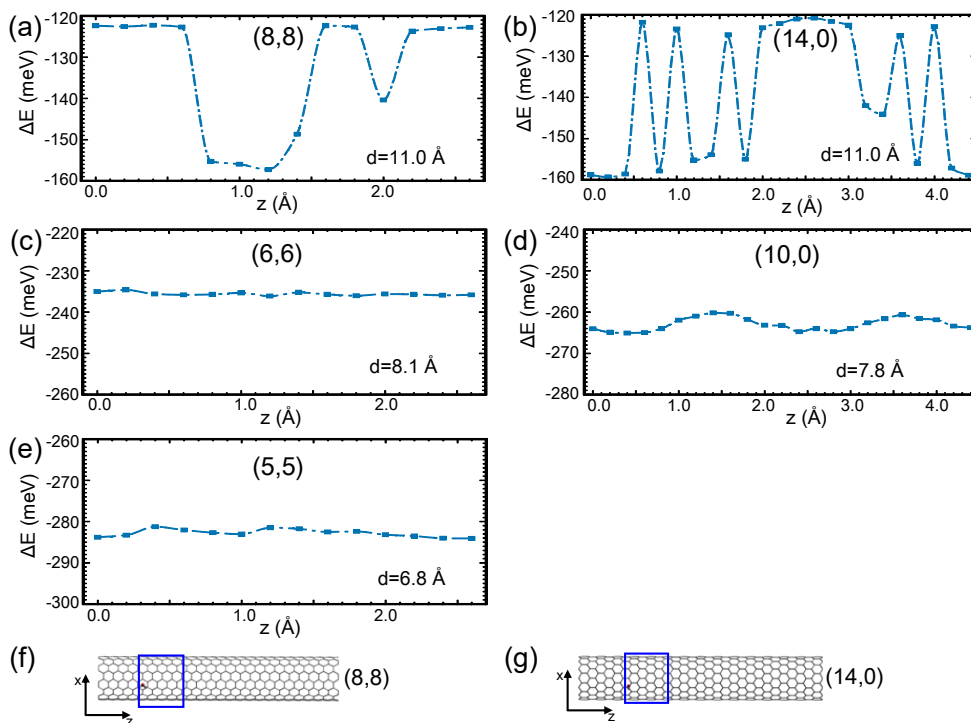


FIG. 3. Interaction energy  $\Delta E(z)$  between an isolated  $\text{H}_2\text{O}$  molecule and a surrounding (a) (8,8), (b) (14,0), (c) (6,6), (d) (10,0), and (e) (5,5) CNT. The  $z$ -coordinate represents the water position along the  $z$ -axis of the CNT. Only the stable water orientation with the hydrogens facing the wall are considered. The range of  $\Delta E(z)$  values is 40 meV in all panels. Schematic geometry is shown for (f) the (8,8) and (g) the (14,0) CNT, with the size of the unit cell considered being outlined by the blue box. Nanotube diameters  $d$  are indicated in the individual panels.

linked to the fact that in very narrow nanotubes, atoms all around the nanotube perimeter interact with the enclosed molecule. While stabilizing the enclosed molecule, it results in frustrated geometries that reduce the dependence of the interaction energy  $\Delta E$  on the position of the molecule  $z$ . This general trend has been identified in published MD simulations based on parameterized force fields [38, 39]. In agreement with our findings, these studies found that slip lengths of water molecules decreased with increasing CNT diameter and asymptotically approached the value for water on planar graphene.

The presented quantitative findings compare well with published DFT-PBE results for the drift of a monolayer of 2D ice on graphene, suggesting energy barriers of  $\approx 15$  meV/ $\text{H}_2\text{O}$  along the zigzag and  $\approx 25$  meV/ $\text{H}_2\text{O}$  along the armchair direction [40]. We note that the strong  $\text{H}_2\text{O}$ - $\text{H}_2\text{O}$  interaction in ice does not allow individual water molecules the same configurational freedom as the geometry considered here.

Our results in Table I also suggest that potential energy barriers  $E_p$  in zigzag CNTs are typically higher by  $\approx 3$  meV than in armchair nanotubes. At this point, we should realize that drift occurs along the armchair direction in CNTs with a zigzag edge and along the zigzag direction in nanotubes with an armchair edge. Even though the small difference between activation barriers approaches the precision limit of PBE-DFT, we are

pleased that our results for a single  $\text{H}_2\text{O}$  molecule match those for 2D ice/graphene [40] quite well. A similar small difference between activation barriers in zigzag and armchair nanotubes, based on MD simulations with parameterized force fields, has been reported previously [41, 42].

We noted another point of interest when studying the passage of a water molecule through a very narrow (5,5) nanotube. Considering the van der Waals diameter  $d_{vdW}(\text{H}_2\text{O}) = 2.8$  Å of a water molecule [43] and the van der Waals radius  $r_{vdW}(\text{C}_{atom}) = 1.8$  Å [44] of a carbon atom, the sum  $d_{vdW}(\text{H}_2\text{O}) + 2r_{vdW}(\text{C}_{atom}) = 6.4$  Å is only 0.5 Å smaller than the diameter  $d = 6.9$  Å of the (5,5) CNT. In other words, this is a rather tight fit for the enclosed molecule. Naïvely, pressing the molecule against the wall should increase the activation barrier for diffusion. In reality, the opposite is true. The molecule now interacts with many atoms along the perimeter of the surrounding nanotube, with unfavorable interactions compensating favorable interactions in different regions. The resulting frustration lowers the activation barriers for diffusion.

### C. Water diffusion inside chiral CNTs

To complete our study of water in CNTs, we present our results for water inside three chiral nanotubes with



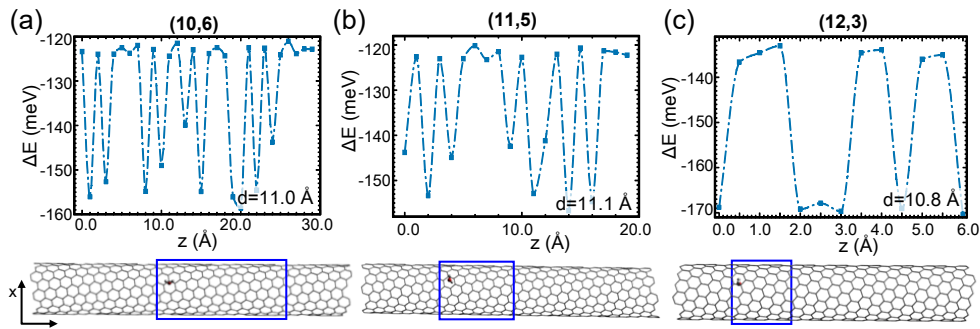


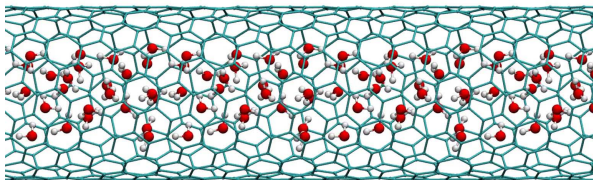
FIG. 4. Interaction energy  $\Delta E(z)$  between an isolated  $\text{H}_2\text{O}$  molecule and a surrounding (a) (10,6), (b) (11,5) and (c) (12,3) CNT. The range of  $\Delta E(z)$  values is 40 meV in all panels. Nanotube diameters  $d$  are indicated in the individual panels. The  $z$ -coordinate represents the water position along the  $z$ -axis of the CNT. Only the stable water orientation with the hydrogens facing the wall are considered. Schematic geometries including the unit cells considered are shown below the respective  $\Delta E(z)$  plots.

a similar diameter  $d \approx 11 \text{ \AA}$  in Fig. 4. We used different step sizes due to the different unit cells, which depend on the chiral index. Our findings of essentially the same energy barrier values  $E_p \approx 30 \text{ meV}$  fall in line with all our other results, suggesting that the energy barriers depend primarily in the nanotube diameter, with only minor dependence on the chiral index.

We have also filled the chiral (12,6) CNT with water and used a DFT-PBE based MD simulation to study the flow driven by pressure difference between the tube ends, which is counter-balanced by drag. As seen in Video 1, the chirality of the surrounding CNT does not exert a sufficient torque on the water column to induce axial rotation.

#### D. Water diffusion inside BNNTs

Similar to graphite, hexagonal boron nitride ( $h$ -BN) is a layered material capable of forming nanotubes [10]. Even though  $h$ -BN is isoelectronic to graphene, B-N bonds are slightly longer than C-C bonds in graphene. There is a corresponding  $\approx 2\%$  increase in the diameter of BNNTs over CNTs with the same chiral index. Unlike CNTs, all BNNTs are wide-gap insulators. The polar nature of the B-N bond provides additional attraction to polar molecules such as water. In analogy to our



Video 1. MD simulation of water flow through a chiral (12,6) CNT.

CNT results, we present the interaction energy of a water molecule with surrounding (8,8) and (14,0) BNNTs in Fig. 5.

Unlike in CNTs of similar diameter, we found optimization of water inside BNNTs to be more demanding, likely due to the long-range nature of the Coulomb interactions dominating there. While we could not guarantee identifying the lowest energy state among many optima with similar energies, our results in Fig. 5 provide consistent trends. For the sake of comparison with the corresponding CNTs, we summed up the van der Waals radii  $r_{vdW}(\text{N}) = 1.55 \text{ \AA}$  of nitrogen [44],  $r_{vdW}(\text{B}) = 1.92 \text{ \AA}$  of boron [45], and the van der Waals diameter  $d_{vdW}(\text{H}_2\text{O}) = 2.8 \text{ \AA}$  of a water molecule [43]. The corresponding diameter of a BNNT that would contain water in a tight fit is  $6.3 \text{ \AA}$ . This value is significantly smaller than the diameter  $d \approx 11 \text{ \AA}$  of (8,8) and (14,0) BNNTs, indicating that – similar to CNTs – the water molecule is not sterically constrained in these nanotubes.

The suggested additional attraction of water to walls of BNNTs in comparison to CNTs is best illustrated by comparing  $\Delta E$  values for  $\text{H}_2\text{O}$  in (8,8) and (14,0) nanotubes of carbon and BN presented in Figs. 3(a-b) and 5. For both chiral indices, we see a significant stabilization of water molecules in BNNTs by  $\approx 40 \text{ meV}$  over CNTs. A naïve expectation of corresponding increase of activation barriers for diffusion has not materialized; we find a similar value  $E_p \approx 40 \text{ meV}$  in all these nanotubes.

The similarity of the activation barriers for water in BNNTs and CNTs has an interesting physical origin. Net charges do not play a major role in the non-polar bond between  $\text{H}_2\text{O}$  and a CNT, with hydrogens facing the wall, which is rather local. The situation is rather different for water inside a BNNT. The Coulomb interaction between the polar  $\text{H}_2\text{O}$  molecule is long-ranged, involving charges on B and N sites all around the BNNT diameter. Whereas the water dipole encounters a net stabilization inside a BNNT, the competition between significant attractive and repulsive forces that are long-ranged leads to a degree of frustration that decreases the dependence

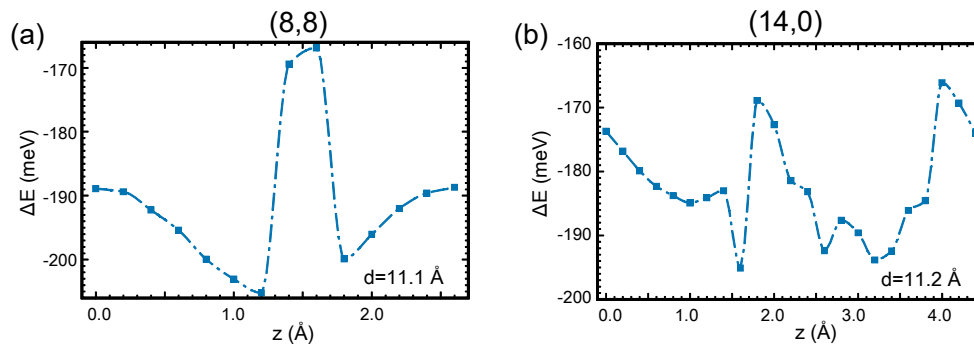


FIG. 5. Interaction energy  $\Delta E(z)$  between an isolated water molecule contained in an (a) (8,8) and (b) (14,0) BNNT. Nanotube diameters  $d$  are indicated in the individual panels. The range of  $\Delta E(z)$  values is 40 meV in all panels. The  $z$ -coordinate represents the position of the molecule along the  $z$ -axis of the BNNT.

of  $\Delta E$  on the axial position of the molecule.

Controversial results have been reported on water flow through CNTs and BNNTs. Results claiming a faster flow of water in BNNTs than in CNTs [46, 47] directly contradict results to the opposite [41, 48, 49].

Setting aside that additional issue of different entry barriers for water in CNTs and BNNTs [50], diffusion barriers for drifting water, which depend on local orbital hybridization with nanotube atoms as well as long-range Coulomb forces, can not be described adequately by parameterized short-range potentials [51, 52], which tend to exaggerate the value of  $E_p$  in BNNTs.

Unlike inside a cylindrical BNNT, there is much less frustration in terms of competing attractive and repulsive forces on planar  $h$ -BN. As evidenced by *ab initio* DFT calculations [53], this leads to an increased modulation of  $\Delta E$  across the  $h$ -BN surface in comparison to graphene.

### E. Diffusion of different molecules inside CNTs

The above-mentioned application of CNTs for the filtration of water can be trivially extended to other liquids, and there is some experimental and theoretical evidence in the direction [11, 29, 54–56]. Besides water, we studied methanol ( $\text{CH}_3\text{-OH}$ , Me-OH) and dimethyl ether ( $\text{CH}_3\text{-O-CH}_3$ , MeOMe) molecules that are comparable in size. All three substances are important solvents, with the dielectric constant decreasing to  $\text{H}_2\text{O}$ , Me-OH, and to MeOMe, as represented in Table II. We studied the potential energy surface  $\Delta E(z)$  for each of these molecules drifting along the (8,8) CNT in much the same way as described for water earlier. Our results for  $\Delta E(z)$  are displayed in Fig. 5 and for the energy barriers  $E_p$  in Table II.

Sequential substitution of hydrogen atoms by methyl groups substantially lowers the dipole moment  $p$  of the molecule and the dielectric constant  $\epsilon$  of the liquid. This lowers the interaction of the molecule with the inner CNT wall and lower diffusion barriers, as seen clearly by comparing our results for  $\text{H}_2\text{O}$  and methanol in Fig. 6. As

seen in Fig. 6(c), this trend is not completely followed by dimethyl ether with a very low static dipole moment.

While increasing the number of hydrogens substituted by methyl groups lowers the dipole moment, the concurrent growth of molecular size increases the molecular polarizability  $\alpha$ , reaching its maximum in dimethyl ether. It may be argued that higher values of  $\alpha$  correlate with higher reactivity and stronger interaction with the tube wall. In comparison to water, we see a similar bonding enhancement, indicated by lower values of  $\Delta E$ , in both methanol and dimethyl ether. Our results suggest that increase in either  $p$  or  $\alpha$  tend to increase the activation barriers for diffusion, which are largest for water and dimethyl ether. We should note that changes in the barrier size are rather modest in the solvents we consider.

TABLE II. Bulk dielectric constant  $\epsilon$ , molecular polarizability  $\alpha$  and energy barrier  $E_p$  for the diffusion of an isolated solvent molecule inside an (8,8) armchair CNT.

Solvent	Dielectric constant $\epsilon$	Polarizability $\alpha$ [57] ( $\times 10^{-24} \text{ cm}^3$ )	$E_p$ (meV)
Water	80.1	1.45	35.0
Methanol	33.0	3.23...3.32	6.9
Dimethyl Ether	6.2	5.16...5.84	12.6

## IV. DISCUSSION

So far, most of our calculations focussed on a single molecule drifting along a CNT or a BNNT. Even though this geometry is different from a nanotube filled with many molecules representing a liquid, a relation between molecular diffusion barriers and the resulting drag force in the liquid has been identified previously [41]. The specific claim, based on MD simulation results for (8,8) and (14,0) CNTs that contain a single  $\text{H}_2\text{O}$  molecule or are filled with water, is that the trends in the friction coefficients are the same in the two cases [41]. Similar to our findings, consistently higher friction coefficients were reported [41] in the zigzag (14,0) CNT than in the armchair

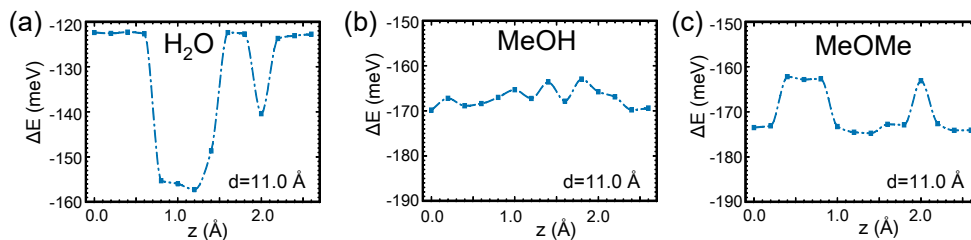


FIG. 6. Interaction energy  $\Delta E(z)$  between an isolated (a) water ( $\text{H}_2\text{O}$ ), (b) methanol ( $\text{CH}_3\text{-OH}$ , MeOH), and (c) dimethyl ether ( $\text{CH}_3\text{-O-CH}_3$ , MeOMe) molecule and a surrounding (8,8) CNT. The range of  $\Delta E(z)$  values is 40 meV and nanotube diameters  $d$  are indicated in all panels. The  $z$ -coordinate represents the position of the molecule along the  $z$ -axis of the CNT.

(8,8) CNT, which contained either a single  $\text{H}_2\text{O}$  molecule or were filled with water. The friction coefficients in the different CNTs were very close in the single-molecule case and increased in size with increasing water filling level.

We believe that the latter finding is closely related to the way, in which activation barriers for diffusion are determined. The potential energy surfaces  $\Delta E(z)$  for different molecules and nanotubes, which we present in our study, are the result of a large number of static constrained structure optimizations. MD simulations of an isolated molecule drifting freely within the nanotube void, on the other hand, will offer a different picture. Even though the potential energy of such a drifting molecule does change along its trajectory, the molecule will unlikely encounter all maxima and minima in the potential energy surface. This would be particularly true for vacancy defects that may not hinder the axial drift of a molecule at finite velocity [58]. Consequently, the spread of potential energies encountered by a freely drifting molecule will be lower than that found in the  $\Delta E(z)$  surfaces presented here.

Molecules in a nanotube completely filled with a liquid are radially constrained by the low compressibility of the liquid and the rigidity of the enclosing CNT wall. In comparison to a freely drifting molecule that barely touches the inner walls, molecules at the interface between the liquid column and the nanotube are forced to ‘hug’ the surface closely, thus probing the potential profile of the nanotube wall more intimately. In general, the liquid column propagates in a plug-like motion along the nanotube [59]. Its viscosity – unlike the friction coefficient – does not contribute much to the friction coefficient [60]. To a small degree, the flexibility of the CNT walls has been shown to further reduce the friction coefficient in comparison to a rigid wall [61, 62].

The calculated relative barriers for the passage of water and other solvents show that the CNT membranes can indeed be used for the separation of liquids and water purification including desalination [7, 8]. Viable applications of aligned CNT membranes may then extend from

removal of organic components from water to the purification of gasoline and other petroleum fractions [56]. The former is an especially pressing issue, since state-of-the-art polymer membranes used in the reverse osmosis process are easily destroyed by hydrocarbons [63]. Polymer membranes also have insufficient selectivity to non-charged organic molecules [64] and are prone to bio-fouling [65–67].

## V. SUMMARY AND CONCLUSIONS

We have conducted *ab initio* DFT studies of the drift of water, methanol and dimethyl ether molecules inside nanotubes of carbon and boron nitride with different diameters and chiral indices. The liquids we choose are important solvents, with water and methanol being polar and dimethyl ether being non-polar. In terms of activation barriers for transport, we find the molecular-level drag to decrease with decreasing nanotube diameter, but to be rather independent of the chiral index. We also found molecules with higher polarity or polarization to experience higher drag during the flow. Rather counter-intuitively, we found the drag for water molecules in boron nitride molecules not exceed that in carbon nanotubes due to frustration in competing long-range Coulomb interactions. We expect that the trends identified in this study may help to design nanotube membranes for the filtration of water and separation of solvents.

## ACKNOWLEDGMENTS

D.T. acknowledges financial support by the NSF/AFOSR EFRI 2-DARE grant number EFMA-1433459. A.K. acknowledges financial support by the Fulbright program. We thank Aleksandr Noy for valuable discussions. Computational resources have been provided by the Michigan State University High Performance Computing Center.

[1] Zhen Zhang, Xiaodong Huang, Yongchao Qian, Weipeng Chen, Liping Wen, and Lei Jiang, “Engineering smart

nanofluidic systems for artificial ion channels and ion

- pumps: From single-pore to multichannel membranes,” *Adv. Mater.* **32**, 1904351 (2020).
- [2] Wan-Qing Yue, Zheng Tan, Xiu-Ping Li, Fei-Fei Liu, and Chen Wang, “Micro/nanofluidic technologies for efficient isolation and detection of circulating tumor cells,” *TrAC, Trends Anal. Chem.* **117**, 101–115 (2019).
  - [3] Sangeeta N. Bhatia and Donald E. Ingber, “Microfluidic organs-on-chips,” *Nat. Biotechnol.* **32**, 760–772 (2014).
  - [4] P Gravesen, J Branebjerg, and O S Jensen, “Microfluidics-a review,” *J. Micromech. Microeng.* **3**, 168–182 (1993).
  - [5] George M. Whitesides, “The origins and the future of microfluidics,” *Nature* **442**, 368–373 (2006).
  - [6] Mateus H. Köhler, José R. Bordin, Carolina F. de Matos, and Marcia C. Barbosa, “Water in nanotubes: The surface effect,” *Chem. Eng. Sci.* **203**, 54–67 (2019).
  - [7] David Tománek and Andrii Kyrylchuk, “Designing an all-carbon membrane for water desalination,” *Phys. Rev. Applied* **12**, 024054 (2019).
  - [8] Yanbing Yang, Xiangdong Yang, Ling Liang, Yuyan Gao, Huanyu Cheng, Xinming Li, Mingchu Zou, Renzhi Ma, Quan Yuan, and Xiangfeng Duan, “Large-area graphene-nanomesh/carbon-nanotube hybrid membranes for ionic and molecular nanofiltration,” *Science* **364**, 1057–1062 (2019).
  - [9] Md. Harun-Or Rashid and Stephen F. Ralph, “Carbon nanotube membranes: Synthesis, properties, and future filtration applications,” *Nanomaterials* **7**, 99 (2017).
  - [10] Nasreen G. Chopra, R. J. Luyken, K. Cherrey, Vincent H. Crespi, Marvin L. Cohen, Steven G. Louie, and A. Zettl, “Boron nitride nanotubes,” *Science* **269**, 966–967 (1995).
  - [11] Samuel Faucher, Narayana Aluru, Martin Z. Bazant, Daniel Blankshtein, Alexandra H. Brozena, John Cummings, J. Pedro de Souza, Menachem Elimelech, Razi Epsztein, John T. Fourkas, Ananth Govind Rajan, Heather J. Kulik, Amir Levy, Arun Majumdar, Charles Martin, Michael McEldrew, Rahul Prasanna Misra, Aleksandr Noy, Tuan Anh Pham, Mark Reed, Eric Schwegler, Zuzanna Siwy, Yuhuang Wang, and Michael Strano, “Critical knowledge gaps in mass transport through single-digit nanopores: A review and perspective,” *J. Phys. Chem. C* **123**, 21309–21326 (2019).
  - [12] Amrit Kalra, Shekhar Garde, and Gerhard Hummer, “(cul-id:1887995) from the cover: Osmotic water transport through carbon nanotube membranes,” *Proc. Natl. Acad. Sci. U.S.A.* **100**, 10175–10180 (2003).
  - [13] Fangqiang Zhu and Klaus Schulten, “Water and proton conduction through carbon nanotubes as models for biological channels,” *Biophys. J.* **85**, 236–244 (2003).
  - [14] John A. Thomas and Alan J. H. McGaughey, “Water flow in carbon nanotubes: Transition to subcontinuum transport,” *Phys. Rev. Lett.* **102**, 184502 (2009).
  - [15] G. Hummer, J. C. Rasaiah, and J. P. Noworyta, “Water conduction through the hydrophobic channel of a carbon nanotube,” *Nature* **414**, 188–190 (2001).
  - [16] Rahul Prasanna Misra and Daniel Blankshtein, “Insights on the role of many-body polarization effects in the wetting of graphitic surfaces by water,” *J. Phys. Chem. C* **121**, 28166–28179 (2017).
  - [17] David J. Mann and Mathew D. Halls, “Water alignment and proton conduction inside carbon nanotubes,” *Phys. Rev. Lett.* **90**, 195503 (2003).
  - [18] Christoph Dellago, Mor M. Naor, and Gerhard Hummer, “Proton transport through water-filled carbon nanotubes,” *Phys. Rev. Lett.* **90**, 105902 (2003).
  - [19] Sofie Cambré, Bob Schoeters, Sten Luyckx, Etienne Goovaerts, and Wim Wenseleers, “Experimental observation of single-file water filling of thin single-wall carbon nanotubes down to chiral index (5,3),” *Phys. Rev. Lett.* **104**, 207401 (2010).
  - [20] Alexander I. Kolesnikov, Jean Marc Zanutti, Chun Keung Loong, Pappannan Thiyagarajan, Alexander P. Moravsky, Raouf O. Loutfy, and Christian J. Burnham, “Anomalously soft dynamics of water in a nanotube: A revelation of nanoscale confinement,” *Phys. Rev. Lett.* **93**, 035503–1 (2004).
  - [21] Yingchun Liu, Qi Wang, Tao Wu, and Li Zhang, “Fluid structure and transport properties of water inside carbon nanotubes,” *J. Chem. Phys.* **123**, 234701 (2005).
  - [22] Kenichiro Koga, G. T. Gao, Hideki Tanaka, and X. C. Zeng, “Formation of ordered ice nanotubes inside carbon nanotubes,” *Nature* **412**, 802–805 (2001).
  - [23] Giancarlo Cicero, Jeffrey C. Grossman, Eric Schwegler, Francois Gygi, and Giulia Galli, “Water confined in nanotubes and between graphene sheets: a first principle study,” *J. Am. Chem. Soc.* **130**, 1871–8 (2008).
  - [24] Oleg Byl, Jin Chen Liu, Yang Wang, Wai Leung Yim, J. Karl Johnson, and John T. Yates, “Unusual hydrogen bonding in water-filled carbon nanotubes,” *J. Am. Chem. Soc.* **128**, 12090–12097 (2006).
  - [25] Yutaka Maniwa, Hiromichi Kataura, Masatoshi Abe, Akiko Uda, Shinzo Suzuki, Yohji Achiba, Hiroshi Kira, Kazuyuki Matsuda, Hiroaki Kadowaki, and Yutaka Okabe, “Ordered water inside carbon nanotubes: Formation of pentagonal to octagonal ice-nanotubes,” *Chem. Phys. Lett.* **401**, 534–538 (2005).
  - [26] J. K. Holt, “Fast mass transport through sub-2-nanometer carbon nanotubes,” *Science* **312**, 1034–1037 (2006).
  - [27] J. Eijkel, “Liquid slip in micro- and nanofluidics: Recent research and its possible implications,” *Lab. Chip.* **7**, 299–301 (2007).
  - [28] Eric Lauga, Michael Brenner, and Howard Stone, “Microfluidics: The no-slip boundary condition,” in *Springer Handbook of Experimental Fluid Mechanics* (Springer Berlin Heidelberg, Berlin, Heidelberg, 2007) pp. 1219–1240.
  - [29] Max Whitby, Laurent Cagnon, Maya Thanou, and Nick Quirke, “Enhanced fluid flow through nanoscale carbon pipes,” *Nano Lett.* **8**, 2632–2637 (2008).
  - [30] Ioannis N. Tsimpanogiannis, Othonas A. Moulton, Luís F.M. Franco, Marcelle B.de M. Spera, Máté Erdős, and Ioannis G. Economou, “Self-diffusion coefficient of bulk and confined water: a critical review of classical molecular simulation studies,” *Mol. Simul.* **45**, 425–453 (2019).
  - [31] Alexander Quandt, Andrii Kyrylchuk, Gotthard Seifert, and David Tománek, “Water flow through a graphite oxide membrane: A phenomenological description,” (Unpublished).
  - [32] Emilio Artacho, E. Anglada, O. Dieguez, J. D. Gale, A. Garcia, J. Junquera, R. M. Martin, P. Ordejon, J. M. Pruneda, D. Sanchez-Portal, and J. M. Soler, “The siesta method; developments and applicability,” *J. Phys. Cond. Mat.* **20**, 064208 (2008).
  - [33] John P. Perdew, Kieron Burke, and Matthias Ernzerhof, “Generalized gradient approximation made simple,” *Phys. Rev. Lett.* **77**, 3865–3868 (1996).



- [34] N. Troullier and José Luís Martins, “Efficient pseudopotentials for plane-wave calculations,” *Phys. Rev. B* **43**, 1993–2006 (1991).
- [35] Hendrik J. Monkhorst and James D. Pack, “Special points for brillouin-zone integrations,” *Phys. Rev. B* **13**, 5188–5192 (1976).
- [36] M.R. Hestenes and E. Stiefel, “Methods of conjugate gradients for solving linear systems,” *J. Res. Natl. Bur. Stand. (U. S.)* **49**, 409 (1952).
- [37] A. Ambrosetti and P. L. Silvestrelli, “Adsorption of rare-gas atoms and water on graphite and graphene by van der waals-corrected density functional theory,” *J. Phys. Chem. C* **115**, 3695–3702 (2011).
- [38] Sridhar Kumar Kannam, B. D. Todd, J. S. Hansen, and Peter J. Davis, “How fast does water flow in carbon nanotubes?” *J. Chem. Phys.* **138**, 094701 (2013).
- [39] Kerstin Falk, Felix Sedlmeier, Laurent Joly, Roland R. Netz, and Lydéric Bocquet, “Molecular origin of fast water transport in carbon nanotube membranes: Superlubricity versus curvature dependent friction,” *Nano Lett.* **10**, 4067–4073 (2010).
- [40] Danil W. Boukhvalov, Mikhail I. Katsnelson, and Young Woo Son, “Origin of anomalous water permeation through graphene oxide membrane,” *Nano Lett.* **13**, 3930–3935 (2013).
- [41] Xingfei Wei and Tengfei Luo, “Effects of electrostatic interaction and chirality on the friction coefficient of water flow inside single-walled carbon nanotubes and boron nitride nanotubes,” *J. Phys. Chem. C* **122**, 5131–5140 (2018).
- [42] Alan Sam, K. Vishnu Prasad, and Sarith P. Sathian, “Water flow in carbon nanotubes: The role of tube chirality,” *Phys. Chem. Chem. Phys.* **21**, 6566–6573 (2019).
- [43] William L. Jorgensen, Jayaraman Chandrasekhar, Jeffrey D. Madura, Roger W. Impey, and Michael L. Klein, “Comparison of simple potential functions for simulating liquid water,” *J. Chem. Phys.* **79**, 926–935 (1983).
- [44] A. Bondi, “van der Waals volumes and radii,” *J. Phys. Chem.* **68**, 441–451 (1964).
- [45] Manjeera Mantina, Adam C. Chamberlin, Rosendo Valero, Christopher J. Cramer, and Donald G. Truhlar, “Consistent van der Waals radii for the whole main group,” *J. Phys. Chem. A* **113**, 5806–5812 (2009).
- [46] Won CY and Aluru NR, “Water permeation through a subnanometer boron nitride nanotube,” *J. Am. Chem. Soc.* **129**.
- [47] M. E. Suk, A. V. Raghunathan, and N. R. Aluru, “Fast reverse osmosis using boron nitride and carbon nanotubes,” *Appl. Phys. Lett.* **92**, 133120 (2008).
- [48] Konstantinos Ritos, Davide Mattia, Francesco Calabrò, and Jason M. Reese, “Flow enhancement in nanotubes of different materials and lengths,” *J. Chem. Phys.* **140**, 014702 (2014).
- [49] Eleonora Secchi, Sophie Marbach, Antoine Niguès, Derek Stein, Alessandro Siria, and Lydéric Bocquet, “Massive radius-dependent flow slippage in carbon nanotubes,” *Nature* **537**, 210–213 (2016).
- [50] Michael Thomas, Ben Corry, and Tamsyn A. Hilder, “What have we learnt about the mechanisms of rapid water transport, ion rejection and selectivity in nanopores from molecular simulation?” *Small* **10**, 1453–1465 (2014).
- [51] T.A. Hilder, R. Yang, V. Ganesh, D. Gordon, A. Bliznyuk, A.P. Rendell, and S.-H. Chung, “Validity of current force fields for simulations on boron nitride nanotubes,” *Micro & Nano Lett.* **5**, 150 (2010).
- [52] Matthew Melillo, Fangqiang Zhu, Mark A. Snyder, and Jeetain Mittal, “Water transport through nanotubes with varying interaction strength between tube wall and water,” *J. Phys. Chem. Lett.* **2**, 2978–2983 (2011).
- [53] Gabriele Tocci, Laurent Joly, and Angelos Michaelides, “Friction of water on graphene and hexagonal boron nitride from ab initio methods: Very different slippage despite very similar interface structures,” *Nano Lett.* **14**, 6872–6877 (2014).
- [54] Lev D. Gelb, K. E. Gubbins, R. Radhakrishnan, and M. Sliwinska-Bartkowiak, “Phase separation in confined systems,” *Rep. Prog. Phys.* **62**, 1573–1659 (1999).
- [55] J. Czwartos, B. Coasne, K. E. Gubbins \*, F. R. Hung, and M. Sliwinska-Bartkowiak, “Freezing and melting of azeotropic mixtures confined in nanopores: experiment and molecular simulation,” *Mol. Phys.* **103**, 3103–3113 (2005).
- [56] A. Srivastava, O. N. Srivastava, S. Talapatra, R. Vajtai, and P. M. Ajayan, “Carbon nanotube filters,” *Nat. Mater.* **3**, 610–614 (2004).
- [57] *CRC Handbook of Chemistry and Physics*, 67th ed. (CRC Press, Boca Raton, FL, USA, 1986).
- [58] Sony Joseph and N. R. Aluru, “Why are carbon nanotubes fast transporters of water?” *Nano Lett.* **8**, 452–458 (2008).
- [59] Itsuo Hanasaki and Akihiro Nakatani, “Flow structure of water in carbon nanotubes: Poiseuille type or plug-like?” *J. Chem. Phys.* **124**, 144708 (2006).
- [60] Laurent Joly, “Capillary filling with giant liquid/solid slip: Dynamics of water uptake by carbon nanotubes,” *J. Chem. Phys.* **135**, 214705 (2011).
- [61] Alan Sam, Sridhar Kumar Kannam, Remco Hartkamp, and Sarith P. Sathian, “Water flow in carbon nanotubes: The effect of tube flexibility and thermostat,” *J. Chem. Phys.* **146** (2017), 10.1063/1.4985252.
- [62] Jiabo Tao, Xianyu Song, Teng Zhao, Shuangliang Zhao, and Honglai Liu, “Confinement effect on water transport in cnt membranes,” *Chem. Eng. Sci.* **192**, 1252–1259 (2018).
- [63] David Jassby, Tzahi Y. Cath, and Herve Buisson, “The role of nanotechnology in industrial water treatment,” *Nat. Nanotechnol.* **13**, 670–672 (2018).
- [64] Vittorio Albergamo, Bastiaan Blankert, Emile Cornelissen, Bas Hof, Willem-Jan Knibbe, Walter van der Meer, and Pim de Voogt, “Removal of polar organic micropollutants by pilot-scale reverse osmosis drinking water treatment,” *Wat. Res.* **148**, 535–545 (2018).
- [65] Jay R. Werber, Chinedum O. Osuji, and Menachem Elimelech, “Materials for next-generation desalination and water purification membranes,” *Nat. Rev. Mater.* **1**, 16018 (2016).
- [66] Jay R. Werber, Akshay Deshmukh, and Menachem Elimelech, “The critical need for increased selectivity, not increased water permeability, for desalination membranes,” *Environ. Sci. Tech. Let.* **3**, 112–120 (2016).
- [67] Menachem Elimelech and William A Phillip, “The future of seawater desalination: Energy, technology, and the environment,” *Science* **333**, 712–717 (2011).